Site-Selective Holographic Imaging of Iron Arrangements in Magnetite

P. Korecki,[1] M. Szymoński,[1] J. Korecki,[2,3] and T. Ślęzak[2]
[1]*Institute of Physics, Jagiellonian University, Kraków, Poland*
[2]*Faculty of Physics and Nuclear Techniques, AGH University of Science and Technology, Kraków, Poland*
[3]*Institute of Catalysis and Surface Chemistry, Polish Academy of Sciences, Kraków, Poland*
(Received 16 February 2004; published 19 May 2004)

Complex γ-ray holograms were recorded by tuning to the nuclear absorption lines of ^{57}Fe in magnetite corresponding to different hyperfine fields. The numerical reconstruction of the holograms to real space provided three-dimensional images of local iron arrangements in octahedral and tetrahedral sublattices of magnetite. This direct site-selective imaging of atomic structure was performed using a tabletop experimental setup.

DOI: 10.1103/PhysRevLett.92.205501 PACS numbers: 61.10.–i, 07.85.–m, 42.40.–i, 61.18.Fs

Most x-ray, electron, and neutron diffraction techniques use both an external radiation source and an external detector. Placing a source or a detector inside the sample, which can be effected by using emitting or absorbing atoms, makes it possible to use Gabor's holographic formalism to analyze the diffraction pattern and overcome the crystallographic phase problem. Recently, holographic methods using such internal sources [1,2] and detectors [3–5] provided three-dimensional images of the local structure in solids. Internal detector holography [6], which we apply here, uses atoms or nuclei within the sample to sense the interference between the external radiation reaching them either directly (the holographic reference wave) or after scattering on nearby atoms (the object waves). Secondary yield emitted from these detectors is then collected as the specimen is rotated relative to the incident beam direction. A holographic formalism [7] is used for a direct transformation [8] of the recorded pattern into a three-dimensional image of the local structure around detecting atoms. By selection of the characteristic radiation emitted from atomic detectors, chemical resolution can be achieved. Holographic methods using x rays and neutrons were unable to distinguish between atoms of the same kind, which occupy nonequivalent crystallographic sites. This ability is provided by γ-ray holography [4] utilizing coherent effects in the Mössbauer nuclear absorption [9], as it gives spectroscopic information, which was pointed out already in the work proposing γ-ray holography [10]. With hyperfine interactions, nuclear detectors can probe internal electromagnetic fields inside the sample and thus provide local spectroscopic information that can be used to distinguish between crystallographic sites having different chemical environments and magnetic properties [11].

In this Letter, by supplementing holographic imaging with a spectroscopic sense, we obtained three-dimensional images of iron arrangements at nonequivalent sites in magnetite. We achieved these site-resolved images from complex γ-ray holograms [12] recorded using a tabletop experimental setup.

In magnetite (Fe_3O_4), which is the oldest known magnetic mineral, iron ions occupy interstitial tetrahedral and octahedral positions with respect to the cubic oxygen lattice of the inverse spinel [13] that is found in magnetite above the Verwey temperature $T_V \sim 125$ K [14]. Tetrahedral A sites are occupied by eight Fe^{3+} ions, whereas octahedral B sites are randomly occupied by eight Fe^{3+} and eight Fe^{2+} ions. Despite several decades of experimental and theoretical studies, intricate magnetoelectronic interactions in magnetite remain incompletely understood [15]. As proposed by Verwey, a thermally activated fast electron hopping between octahedral Fe^{3+} and Fe^{2+} ions is responsible for high conductivity above T_V. However, this simple model was recently questioned and is still being modified [16,17]. An important contribution to understanding the electronic and magnetic structure of magnetite has been made by the Mössbauer spectroscopy.

The Mössbauer spectrum of our epitaxial thin film sample is shown in Fig. 1(a). It consists of two Zeeman sextets, which are differently split by the internal magnetic fields and have different chemical shifts [18]. The common interpretation, based on the Verwey model, is that the first sextet with the larger splitting corresponds to Fe^{3+} ions at A sites and the second one to Fe cations with an average valency of 2.5+ at B sites [18]. However, one could also expect that both Fe^{3+} ions at different lattice sites have similar hyperfine interaction parameters as it is observed below T_V or in γ-Fe_2O_3 [9]. Therefore, magnetite is a good model system for a new type of an experiment, in which atomic arrangements can be directly imaged with the site resolution and which for the first time directly explains the origin of the subcomponents of the Mössbauer spectrum.

Our experiment combines γ-ray holography with the capabilities of Mössbauer spectroscopy and diffraction [19,20]. The idea is to tune to the best resolved lines of the magnetite subspectra shown in Fig. 1(a), and to record separate holograms for both transitions. Since the nuclear levels are extremely narrow, both absorption on

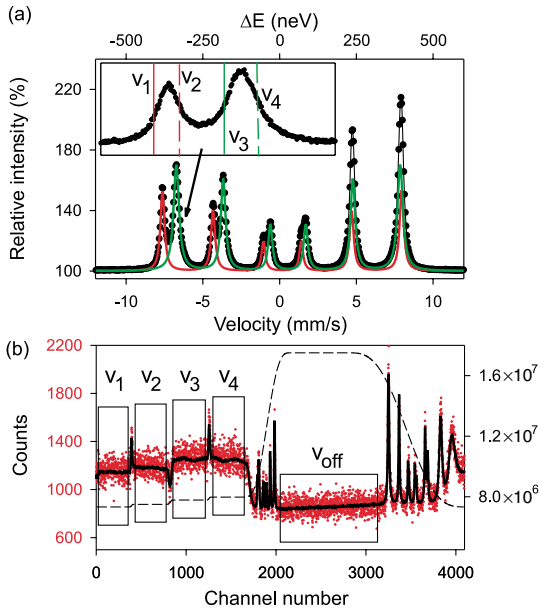

FIG. 1 (color online). Acquisition of complex γ-ray holograms for $^{57}Fe_3O_4$. (a) Conversion electron Mössbauer spectrum of $^{57}Fe_3O_4$ epitaxial film recorded before experiment. The spectrum consists of two Zeeman sextets corresponding to Fe^{3+} ions and Fe ions with effective valency 2.5 +, respectively. Points represent measured data; lines are fits to the experimental data. The inset shows an enlarged view of best resolved lines indicated by an arrow. Complex γ-ray holograms were recorded by detuning below and above exact resonances (as depicted by solid and dashed lines, respectively) to achieve a shift of the scattering phase. (b) The holograms were acquired simultaneously using the velocity signal shown as a dashed line (not to scale). Points represent conversion electron yield recorded for a single sample orientation. The sum of counts in the regions of well-defined constant velocities, indicated by rectangles, were taken as single points of two-dimensional holograms. The spectrum summed over all orientations is represented by a solid line. The left and right horizontal scales refer to points and solid line, respectively

the detecting nucleus and nuclear resonant scattering on neighboring nuclei occur only when the involved nuclei are at equivalent sites. A serious problem for all single energy holographies is twin images [21]. Twin images destructively add to the real images and cause the disappearance of certain nuclear images in real-space reconstruction. The problem of the twin images was solved recently by complex holography [12], which takes advantage of the shift of the scattering phase by detuning from the resonance [22]. Unambiguous structural information can be obtained from the difference (so-called real hologram) and the sum (imaginary hologram) of the patterns symmetrically recorded below and above the resonance. Therefore, two holograms have to be recorded for each transition.

For the present experiment, we prepared a 200 nm epitaxial film of $^{57}Fe_3O_4$ on a MgO(001) substrate (10×10 mm^2)—a nuclear resonant experiment with iron requires usage of a ^{57}Fe isotope, which has only 2.17% abundance. The film revealed a grainy structure, which together with its small thickness reduced multiple scattering and extinction effects [23] that could spoil the holograms. The stoichiometry of the sample was monitored during the experiment. Some minor surface oxidation of the film was detected, resulting in the creation of Fe vacancies in the octahedral sublattice.

The experimental setup was a dedicated angular resolved conversion electron Mössbauer spectrometer. We used γ rays with energy $E = 14.41$ keV ($\lambda = 0.86$ Å) from a 150 mCi radioactive ^{57}Co source (4 mm diameter). In order to tune to a particular energy, the source was placed on an electromechanical transducer coupled to a sophisticated electronic control system. A driving signal consisting of five constant velocity ranges was fed to the transducer. Four velocities were adjusted to the above and the below resonance conditions for both transitions; the fifth velocity corresponded to the off-resonance condition [Fig. 1(b)]. The signal had a smooth shape in order to minimize the mechanical instabilities of the system. For the same reason, the working frequency was kept very small ($\sim$1 Hz). The high number of channels (4096), resulting in high resolution, allowed precise tuning to a selected energy at a given transition. During the whole measurement, only minor drifts of the velocity were observed and corrected online. The spectrum summed over all orientations [Fig. 1(b)] reveals the high stability of the system. The sums of counts in the regions of well-defined constant velocities (normalized by the number of channels in each region) were taken as single points of five two-dimensional patterns. These patterns were additionally multiplied by constant correction factors resulting from changes in the solid angle during motion of the source (the amplitude of the source vibration was $\sim$4 mm).

The sample was fixed inside a conversion electron detector positioned 17.5 cm from the source and rotated on a two angle goniometer relative to the incident beam direction. The measurement was performed for 239×65 orientations covering the hemisphere up to a polar angle of 60° (as measured from the sample surface normal). The acquisition off all patterns took 4.6 months. The acquisition time was much longer than for x-ray holography using synchrotron beams [6]. However, the experiment is tabletop and the high energy resolution of $\Delta E/E \sim 5 \times 10^{-13}$ (for x rays $\Delta E/E \sim 10^{-4}$) allows site selectivity. The measurement was terminated once the fourfold symmetry, expected for the (001)-oriented magnetite film, was recognized in the strongest pattern. On average, 2.5×10^5 counts were collected for each sample orientation and for each velocity. Holograms were extracted from the raw data in the following main steps: (i) Off-resonant counts were subtracted from the patterns; (ii) the sum (imaginary holograms) and difference (real holograms) patterns were combined for both transitions; (iii) a slowly varying background was subtracted (the

difference holograms were almost background-free); finally, (iv) a fourfold symmetrization was performed.

Figure 2 shows the resulting holograms. They are noisy (signal-to-noise ratio ~ 1); however, symmetry directions of the sample can easily be identified. Individual holograms show entirely different features. This indicates that the patterns come from nuclear resonant scattering and not from the electronic Rayleigh one. Prior to the γ-ray experiments, we measured an x-ray hologram in a similar experimental geometry but using synchrotron radiation. Based on this measurement, we could directly exclude that γ-ray holograms are significantly influenced by x-ray scattering and extinction [23] both in the film and in the substrate. In addition, for the difference γ-ray holograms the electronic scattering contribution is removed automatically (for ideal symmetrical detuning), while for the sum holograms a significant part of the electronic scattering contribution was removed by the subtraction of the off-resonance counts.

The real-space reconstruction was performed using Barton's algorithm [8] separately for real and imaginary holograms extended to the full Ewald sphere [24]. Since nuclei are point scatterers for the 14.41 keV radiation, γ-ray holography almost ideally fulfills the assumptions of this algorithm. Real-space images are presented in Fig. 3 [25]. Because of real and twin image cancellation, the reconstructions of real and imaginary holograms reveal different nuclei. However, their combinations properly visualize the ionic arrangements corresponding to the expected positions in the two Fe sublattices of the inverse spinel to within 0.15 Å with spatial resolution of 0.6 Å. Since there are two equivalent orientations of the local environment for A sites and four equivalent for B sites, the reconstruction shows linear combinations of all the environments. Nuclei imaged by real and imaginary holograms are shown using different color scales to underline that these holograms are formed in scattering processes having different phase shifts. The phase shift tuning is a unique feature of any resonance scattering, and

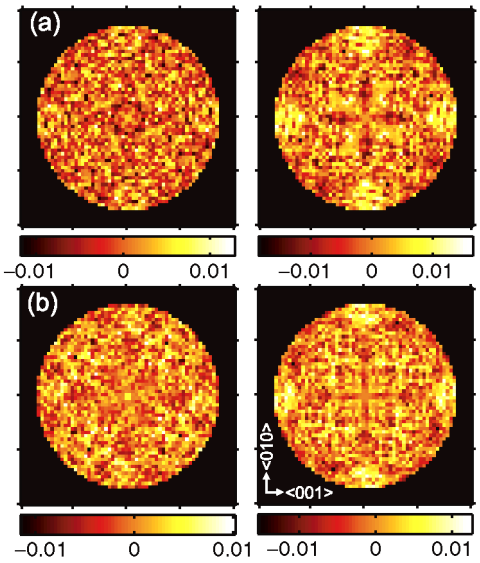

FIG. 2 (color online). Complex γ-ray holograms of Fe_3O_4. Holograms were extracted from two-dimensional patterns of conversion electron yield dependence measured as the sample was rotated relative to the incident γ-ray beam direction. The holograms were obtained for nuclear resonances characteristic of Fe^{3+} (a) and $Fe^{2.5+}$ (b) ions. Left: Real holograms (difference of patterns recorded above and below the resonance). Right: Imaginary holograms (sum of patterns recorded above and below the resonance). The intensity scale is normalized to the nuclear resonant background of each transition. All patterns are presented in the k-vector space as orthographic projections. The ticks are separated by $k/2$, where $k = 2\pi/\lambda = 7.29$ Å^{-1}. A fourfold symmetrization was applied to all patterns.

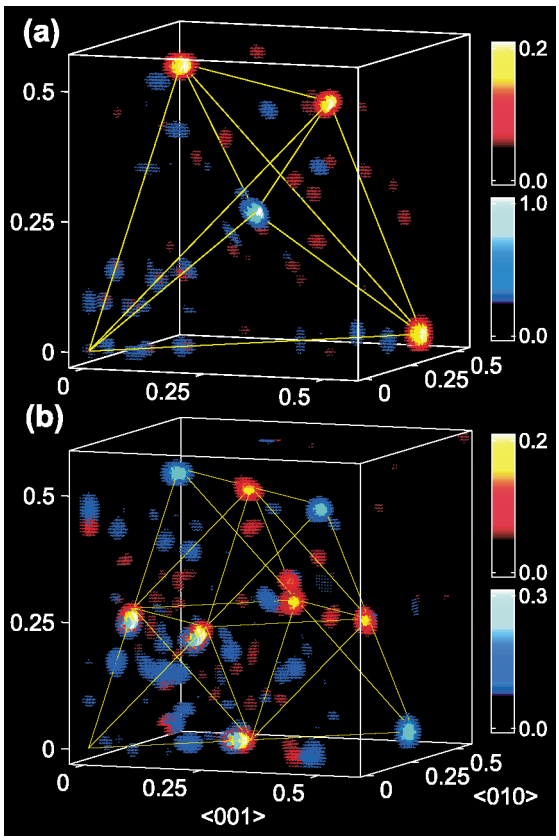

FIG. 3 (color). Three-dimensional real-space images of iron arrangements in magnetite. For clarity, only single octants of the real space are shown. Images were reconstructed from the holograms recorded for the nuclear resonance characteristic of Fe^{3+} (a) and $Fe^{2.5+}$ ions (b). Each of the reconstructed voxels is represented by a small sphere with diameter and color scale proportional to the square of the reconstructed real-space image. The color bars are shown next to plots. The hot color scale corresponds to images reconstructed from real holograms, while the cold color scale to images reconstructed from imaginary holograms. Coordinates are labeled in units of lattice constant ($a_0 = 8.396$ Å). The lines join the expected positions of iron nuclei at A and B sites, respectively, assuming a linear combination of two equivalent A and four B sites, which have different orientations. The reference nuclei (not self-imaged) are located at the origins.

this once again proves the pure nuclear origin of holograms. The reconstruction is shown without any correction for intensities; thus, the visibility of nuclear images does not directly correspond to the expected occupation of the sites. Factors which most strongly influence the intensities in real space are the radial decrease of the scattered waves, finite angular resolution, background subtraction [26], and slightly nonsymmetrical detuning from the resonance. The visible ghost images come from noise, limitations of the single energy reconstruction, and from imperfect background removal. The small shifts of nuclear images arise from the radial falloff of the scattered waves and from errors in the sample orientations. The positions of nuclear images were not significantly influenced by the symmetrization and background subtraction. However, the intensity ratio between the true images and artifacts depended significantly on background removal. There is no mixing of nuclear images of both sublattices. This directly confirms that one Mössbauer subspectrum corresponds to Fe ions at the A sites, while the other one to Fe ions at B sites, which is quite evident but has never been proven before by a direct method.

The foundations of the presented experiment were described earlier [27]. The measured holograms differ from the holograms simulated in that study mainly due to the contribution from further scatterers which was not included in the calculation and due to the nonperfect symmetrical detuning from the resonances. The reconstructed real-space images agree well with the images resulting from simulations; however, small discrepancies resulting from imperfect detuning from the resonances can also be observed.

In this Letter, we experimentally demonstrated that complex γ-ray holography can be used for site-selective imaging of atomic structure. For an unknown system, γ-ray holography can be combined with x-ray holography, which can provide high-quality images of the structure, including oxygen environments as reported recently [28]. For systems containing Mössbauer isotopes, after x-ray holograms are recorded, γ rays can be used to resolve the nonequivalent sites. Here, in order to demonstrate full capabilities of γ-ray holography, we reconstructed complex holograms. For compounds where electronic scattering is dominant, one could be restricted to the recording of only background-free real holograms, whereas for less enriched samples to the recording of one-dimensional profiles and to an error-trial analysis. γ-ray holography is limited by the source intensity, but the use of nuclear resonant scattering beam lines at synchrotrons [29] would remove this restriction. Systems, which are suited for analysis with γ-ray holography, are thin films of multicomponent alloys, buried interfaces, and superlattices which, in order to provide measurable signals must be highly enriched with Mössbauer isotopes. For such systems, if their geometric structure is known beforehand, γ-ray holography can be used to directly correlate their geometric structure with hyperfine interaction parameters.

P. K. acknowledges the cooperation and help of Professor Gerhard Materlik. Dr. Dimitri Novikov is acknowledged for assistance in the synchrotron experiment. This work was supported by Polish State Committee for Scientific Research (Grant No. 5 P03B 069 21) and the Volkswagen Foundation, Federal Republic of Germany.

[1] G. R. Harp, D. K. Saldin, and B. P. Tonner, Phys. Rev. Lett. **65**, 1012 (1990).
[2] M. Tegze and G. Faigel, Nature (London) **49**, 380 (1996).
[3] T. Gog *et al.*, Phys. Rev. Lett. **76**, 3132 (1996).
[4] P. Korecki, J. Korecki, and T. Slezak, Phys. Rev. Lett. **79**, 3518 (1997).
[5] L. Cser *et al.*, Phys. Rev. Lett. **89**, 175504 (2002).
[6] G. Faigel and M. Tegze, Rep. Prog. Phys. **62**, 355 (1999).
[7] A. Szöke, AIP Conf. Proc. **147**, 361 (1986).
[8] J. J. Barton, Phys. Rev. Lett. **61**, 1356 (1988).
[9] N. N. Greenwood and T. C. Gibb, *Mössbauer Spectroscopy* (Chapman and Hall, London, 1971).
[10] M. Tegze and G. Faigel, Europhys. Lett. **16**, 41 (1991).
[11] G. Schatz and A. Weidinger, *Nuclear Condensed Matter Physics: Nuclear Methods and Applications* (Wiley, Chichester, 1996).
[12] P. Korecki, G. Materlik, and J. Korecki, Phys. Rev. Lett. **86**, 1534 (2001)
[13] M. E. Fleet, Acta Crystallogr. Sect. B **37**, 917 (1981).
[14] E. J. W. Verwey, Nature (London) **144**, 327 (1939).
[15] F. Walz, J. Phys. Condens. Matter **14**, R285 (2002).
[16] P. Novak *et al.*, Phys. Rev. B **61**, 1256 (2000).
[17] J. Garcia *et al.*, Phys. Rev. B **63**, 054110 (2001).
[18] R. Bauminger *et al.*, Phys. Rev. **122**, 1447 (1961).
[19] P. J. Black and I. P. Duerdoth, Proc. Phys. Soc. **84**, 169 (1964).
[20] B. Fultz *et al.*, Phys. Rev. B **65**, 064419 (2002).
[21] P. M. Len *et al.*, Phys. Rev. B **50**, 11 275 (1994) .
[22] P. Korecki, J. Korecki, and W. Karas, Phys. Rev. B **59**, 6139 (1999)
[23] P. Korecki, D. V. Novikov, M. Tolkiehn, and G. Materlik, Phys. Rev. B (to be published).
[24] M. Tegze *et al.*, Phys. Rev. Lett. **82**, 4847 (1999).
[25] See EPAPS Document No. E-PRLTAO-92-041419 for auxiliary images. A direct link to this document may be found in the online article's HTML reference section. The document may also be reached via the EPAPS homepage (http://www.aip.org/pubservs/epaps.html) or from ftp.aip.org in the directory /epaps/. See the EPAPS homepage for more information.
[26] G. R. Harp *et al.*, J. Electron Spectrosc. Relat. Phenom. **57**, 331 (1991).
[27] P. Korecki and M. Szymonski, Surf. Sci. **507–510**, 422 (2002).
[28] M. Tegze *et al.*, Nature (London) **407**, 38 (2000).
[29] G. V. Smirnov, Hyperfine Interact. **91**, 125 (2000).